Asymmetric Chemical Functionalization of Top-Contact Electrodes: Tuning the Charge Injection for High-Performance MoS2 Field-Effect Transistors and Schottky Diodes

Bin Han, Yuda Zhao, Chun Ma, Can Wang, Xinzi Tian, Ye Wang, Wenping Hu, Paolo Samorì

DOI: 10.1002/((please add manuscript number))
Article type: Research Article

Asymmetric Chemical Functionalization of Top-Contact Electrodes: Tuning the Charge Injection for High Performance MoS_2 Field-Effect Transistors and Schottky Diodes

*Bin Han, Yuda Zhao, Chun Ma, Can Wang, Xinzi Tian, Ye Wang, Wenping Hu, Paolo Samorì**

B. Han, Prof. Y. Zhao,[+] Dr. C. Ma, Dr. C. Wang, Dr. Y. Wang, Prof. P. Samorì
Université de Strasbourg, CNRS, ISIS
8 allée Gaspard Monge
67000 Strasbourg, France
E-mail: samori@unistra.fr

X. Tian, Prof. W. Hu
Tianjin Key Laboratory of Molecular Optoelectronic Sciences, Department of Chemistry, School of Science, Tianjin University & Collaborative Innovation Center of Chemical Science and Engineering, Tianjin 300072, China

[+] Present address: School of Micro-Nano Electronics, Hangzhou Global Scientific and Technological Innovation Centre, Zhejiang University, 38 Zheda Road, Hangzhou, 310027, China

Keywords: Self-assembled monolayer, Charge injection, Schottky barrier, top-contact bottom-gate, rectification

Abstract: The fabrication of high-performance (opto-)electronic devices based on ultrathin two-dimensional channel materials requires the optimization of the charge injection at the electrode - semiconductor interface. While the chemical functionalization with chemisorbed self-assembled monolayers has been extensively exploited to adjust the work function of metallic electrodes in bottom-contact devices, such a strategy was never demonstrated when the top-contact configuration is chosen, despite the latter is known to offer enhanced charge injection characteristics. Here, we have developed a novel contact engineering method to functionalize gold electrodes in top-contact field-effect transistors (FETs), via the transfer of chemically pre-modified electrodes. The source and drain electrodes of the molybdenum disulfide (MoS_2) FETs were functionalized with prototypical thiolated molecules possessing by design different dipole moments. While the modification of the Au electrode with electron-donating molecules yielded a marked improvement of the device performance, the asymmetric functionalization of the source and drain electrodes with two different chemisorbed molecules with opposed dipole moment enabled the fabrication of a high-performance Schottky diodes with a rectification ratio of ~10^3. Our unprecedented strategy to tune the charge injection and extraction in in top-contact MoS_2 FETs is of general applicability for the fabrication of high-performance opto-electronic devices based on 2D semiconductors in which the energetic asymmetry is required to boost the device functionality (e.g., for light-emitting transistors, solar cells, etc), enabling to tailor the device characteristics on-demand.

Two-dimensional transition metal dichalcogenides (TMDCs) display a broad variety of outstanding electrical and optical properties making them ideal components for the next generation high-performance (opto)electronic devices.[1] Among them, MoS_2 represents a prototypical 2D semiconductor as it combines several advantages such as a sizeable band gap, high I_{on}/I_{off} ratio, great scalability and immunity to short-channel effects.[1a,2] Although MoS_2 based field-effect transistors (FETs) showed good key performance indicators, the currently developed devices are far from exploiting the full potential of this semiconducting material. Major bottlenecks are associated to fundamental physical processes due to the presence of large Schottky barrier heights (SBH, Φ_{SB}), severe Fermi level pinning (FLP) and interfacial defects. In order to boost the device performance charge injection and extraction at the metal - MoS_2 interface need to be optimized.[3] Numerous attempts have been made by using van der Waals (vdW) contacts[4], low work function (WF) contacts[5], insertion of h-BN tunneling layer or metal oxide layer[6], introduction of graphene[7], contact doping[8], and via the functionalization of the electrodes with self-assembled monolayers (SAMs)[3b,9] in devices based on bottom-contact geometries. Among them, SAMs functionalization has been proved to be a powerful and versatile method to adjust the WF of noble metals (Au, Ag, etc.) by reducing the SBH and contact resistance hence improving the carrier injection.

Among various configurations, FETs with bottom-contact geometries are the most commonly used. While they allow easy functionalization of the metallic electrodes with chemisorbed SAMs, they are far from being ideal for high-performance devices. Conversely, both theory[10] and experiments[10b,11] have unambiguously demonstrated that the top-contact configuration of staggered architecture offers better contacts and more efficient charge injection. This can be understood in view of some geometrical reasons: the injection of the coplanar architecture occurs from the contact edge into semiconductor, and all contact area facing the gate of staggered architecture can participate to the injection process.[10c,12] However, the top electrode is generally prepared by thermal deposition, hence it can hardly be chemically modified. On the other hand, deposition of metallic electrodes via the direct vacuum sublimation of “hot” metal atoms onto a molecular surface can be extremely invasive by destroying the molecular layer, leading to short circuits.[13] Moreover, the electrodes functionalization in bottom-contact devices still has some problems which are hard to be overcome. In the first place, due to the metal electrode strong electrostatic screening effect[14], the carrier injects from the contact edge of the electrodes which is limited by the thickness of the electrodes.[12a] Although in principle this can be improved by increasing the electrode thickness, another study demonstrates that the injection efficiency is not proportional to the

thickness of the electrodes: When the electrode becomes thicker, the injection efficiency deteriorates.[15] Furthermore, since the semiconductor layer needs to be prepared after the functionalization of the electrode, the morphology and stacking structure of functionalized molecules have a significant influence on the formation of the semiconductor layer.[16] Therefore, generally applicable methods for fabricating top-contact FETs with functionalized electrodes are nowadays highly sought after.

Herein, we have devised an unprecedented dry-transfer approach enabling the efficient covalent functionalization of top-contacts in MoS_2 based FETs devices. The electrodes are pre-functionalized with SAMs and physically laminated on the 2D semiconductor through vdW contact. The device performance can be tuned via the controlled electrodes functionalization with different chemisorbed SAMs to decrease (increase) the charge injection barrier. This strategy also enables the asymmetric functionalization of the source and drain top-contacts with molecules possessing opposite dipoles, to fabricate Schottky diodes with a rectification ratio exceeding 10^3.

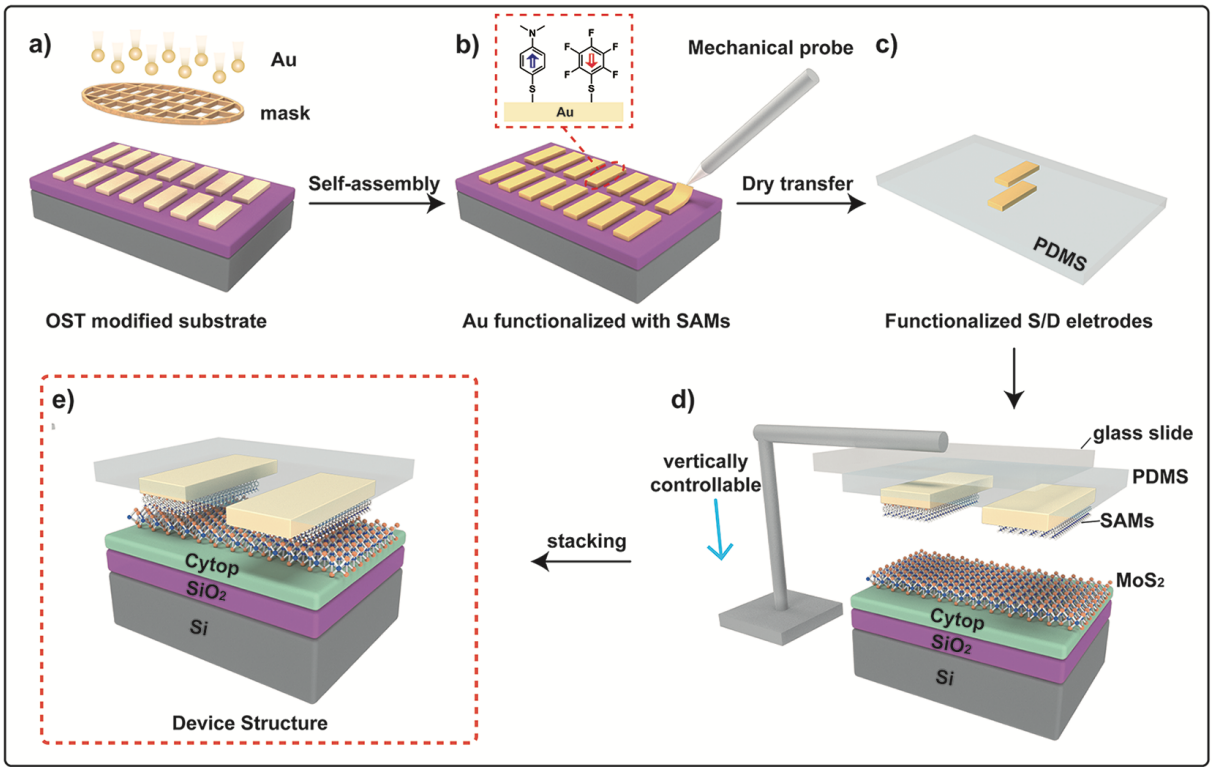

Figure 1. Schematic illustration of the procedure steps for the preparation of top-contact FETs devices with functionalized electrodes. a) Gold evaporation, b) functionalization via SAMs chemisorption, and c) transfer of functionalized electrodes onto PDMS mold. d) Dry transfer and lamination of functionalized electrodes from the mold onto the MoS_2 flake. e) Scheme of FETs structure with SAMs functionalized electrodes. Inset in b) Chemical structure of the thiolated molecules (DABT and PFBT) used in this study. The dipole moment orientation within the molecules is indicated with colored arrows.

The back-gate top-contact MoS_2 FETs were developed with transferred top functionalized Au electrodes by making use of a novel dry transfer technique. The fabrication process is portrayed in Figure 1 (see Supporting Information for fabrication details). A patterned electrode array was first evaporated onto an octadecyltrichlorosilane (OTS) functionalized sacrificial silicon substrate through a copper shadow mask. These patterned electrodes are then functionalized with thiolated molecules after the UV/ozone cleaning treatment. Subsequently, these functionalized electrodes can be mechanically desorbed from the silicon, then dry transferred and laminated on a polydimethylsiloxane (PDMS) surface to form an interelectronic gap using a mechanical probe.[17] The MoS_2 flakes were mechanically exfoliated and transferred to the top of highly doped silicon (p++) covered with a 270 nm thick SiO_2 layer and an insulating spin-coated polymer layer (Cytop, 85 nm) as dielectrics. Compared with conventional Si/SiO_2 interface, the Cytop film represents an ideal substrate for 2D semiconductor, because of its low surface energy, nearly free trap states, absence of dangling bonds and low permittivity ($\varepsilon = 2.1$).[18] Finally, the previously prepared PDMS film exposing functionalized electrodes are aligned under a microscope and physically laminated on the top of the MoS_2 flake, resulting in a top-contact FETs device with functionalized electrodes. The PDMS film is then kept on the top of the device for suitable encapsulation and protection of the device.[19]

The thickness of MoS_2 flakes was monitored by atomic force microscope (AFM) and Raman spectroscopy. Figure S1 and S2 display the morphology and Raman as well as photoluminescence (PL) spectra of MoS_2 flake. We have used MoS_2 flakes with the thickness of 8∼12 nm (12∼19 layers) since such multilayered flakes are robust and they exhibit negligible flake-to-flake variation in the electron affinity and carrier mobility, as well as a low sensitivity to environment. The latter is key since our use of SAMs coated electrodes is aimed at modifying the WF of the electrode rather than at chemically modulating the local electronics of the MoS_2 layers via dipole induced doping or charge transfer.[4,20] Figure 1e shows the architecture of the functionalized FETs device. These top (functionalized-) electrodes and 2D semiconductor are in contact and interacting uniquely via vdW forces. The latter has several advantages such as a lower FLP effect, reduction of the defect-induced gap states and suppression of the metal-induced gap states.[21] The dry transfer technique also possesses unparalleled advantages including the possibility to transfer (functionalized-) electrodes creating a damage-free interface when compared with the more invasive conventional thermal deposition. On the other hand, compared with traditional functionalized bottom-contact configuration, the SAMs in this top-contact configuration is only used to modify the top metal electrode, and have negligible

influence on the semiconductor's structure and electronics.[12a,22] Therefore, the devices characteristics resulting from the exposure to various SAMs functionalized electrodes can be directly correlated to the dipole induced changes in the electron injection barriers, which is also known as SBH (Φ_{SB}). According to the Schottky-Mott rule, the barrier height is defined as the potential difference between WF of the (functionalized-) electrode (W_f) and the electron affinity (χ, defined as the difference between the semiconductor conduction band edge and the vacuum level) of multilayer MoS_2 semiconductor, that is,

$$\Phi_{SB} = W_f - \chi \quad (1)$$

Unfortunately, due to severe FLP, the Schottky–Mott model is not applicable experimentally.[23] In this case, the electron SBH can be characterized by introducing pinning factor (S) and charge neutrality level (CNL, Φ_{CNL}).

$$\Phi_{SB} = S\left(W_f - \Phi_{CNL}\right) + (\Phi_{CNL} - \chi) = S \cdot W_f + b \quad (2)$$

The S was defined as the slope,

$$S = \mathrm{d}\Phi_{SB}/\mathrm{d}W_f \quad (3)$$

The S was varied from 0 for perfect FLP to 1 for no FLP. For MoS_2, a severe FLP effect of $S = 0.02 \sim 0.11$ has been reported by evaporating various metal electrodes.[6a,23a] In view of this, MoS_2 exhibits electron transport behavior.

The characterization of the chemically functionalized electrodes was carried out prior to their transfer. To assess the monolayer morphology, we performed atomic force microscopy (AFM) imaging and contact angle (CA) measurements (see Figure S3 and S4). The root-mean-square (R_{RMS}) roughness of evaporated Au as determined on an area of 2 × 2 μm^2 amounts to 2.05 nm. After functionalization with 4-(dimethylamine)benzenethiol (DABT) and 2,3,4,5,6-pentafluorobenzenethiol (PFBT) chemisorbed SAMs, it slightly changed to 1.98 nm and 2.37 nm, respectively. Such functionalization is also accompanied by a change in the CA from the 77.6 ° of bare electrode to the 86.7° and 58.0° of the PFBT and DABT coated films, respectively. DABT and PFBT, whose chemical structure is displayed in Figure 1b, were chosen as prototypical thiolated molecules because they are rigid and shape persistent and are either strong electron-donor or acceptor. The short contour length along the molecular backbone simply comprising a benzene ring not only ensures good electrical conductivity and sufficient thermal stability, but also minimizes additional tunneling barriers between MoS_2 and metal electrode.[24] The strong dipoles allow to modify the Au electrodes WF of a magnitude as high as 0.7 eV. In particular, the DABT molecule with its lone electron pair shifts the WF of Au electrode from 5.00 eV to 4.30 eV, while the fluorine-rich PFBT molecule increased it to 5.67 eV (see table S1 as well as Figure 3g), as determined by Photoelectron Yield Spectroscopy in

Air (PYSA). The unfunctionalized electrodes were utilized as a reference in the control experiment.

The chemical composition of the electrodes assembled with the DABT and PFBT molecules can be directly analyzed by X-ray Photoelectron Spectroscopy (XPS). Figure S5 shows the C 1s, S 2p, N 1s and F 1s spectra of modified electrodes and compared to the bare electrode. The C 1s peaks of DABT monolayer exhibit the typical C-C bond and C-N bond at 284.8 eV and 285.3 eV, respectively. Similarly, PFBT monolayer displays the C-C bond and C-F bond at 284.8 eV and 286.7 eV, respectively. A clear single symmetric peak of N 1s (at 399.7 eV) and F 1s (at 686.9 eV) provide unambiguous evidence for the formation of the monolayer, by indicating the presence of DABT and PFBT molecules, respectively.[25] In addition, S 2p core level spectrum of SAMs showed only one doublet peak at 162.1 eV corresponding to S chemisorbed onto the gold surface through a thiolate bond.[26]

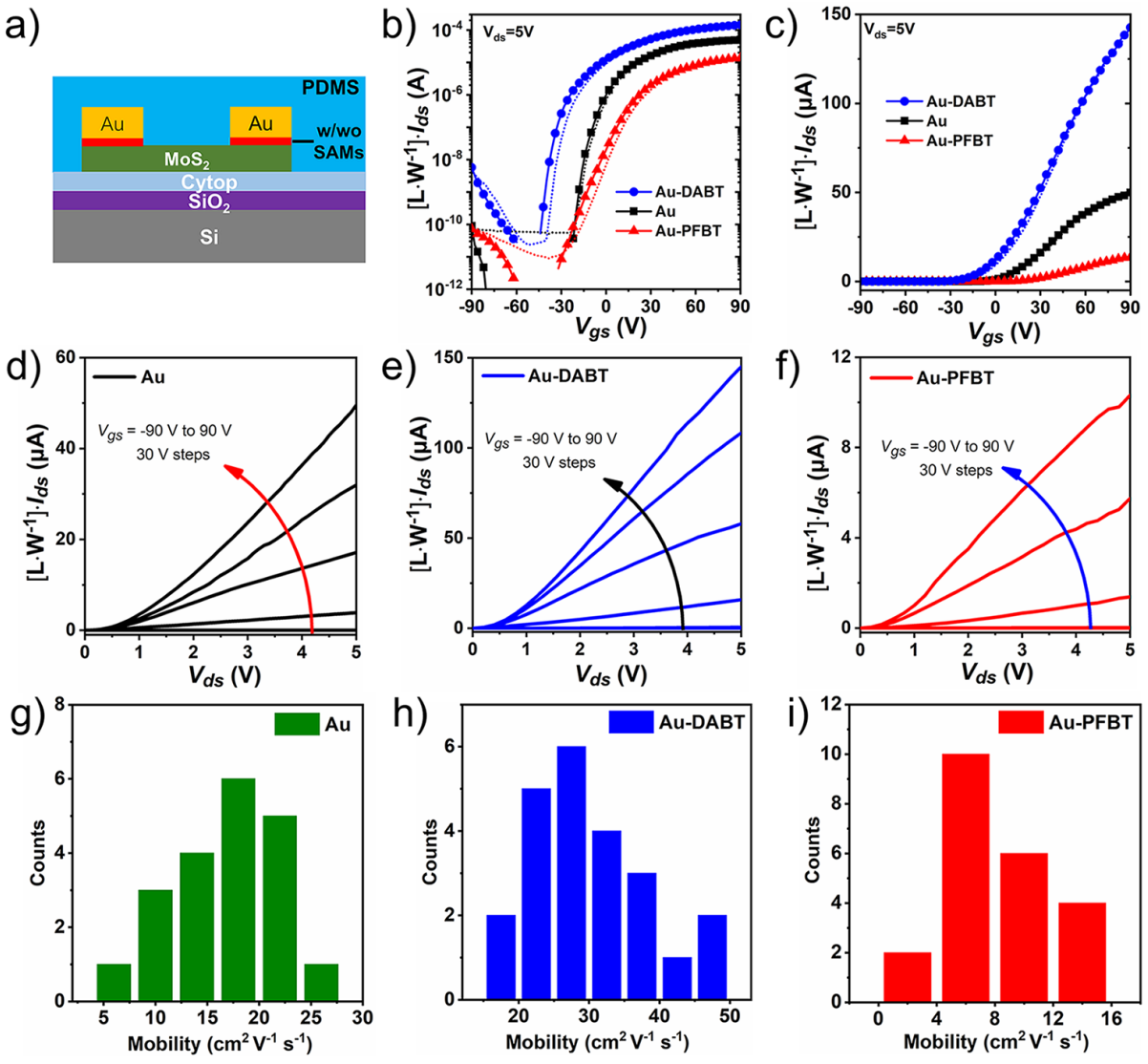

Figure 2. a) Scheme of top-contact FETs with functionalized electrodes structure. (b-i) Comparison of MoS_2 top-contact FETs with bare Au electrode and SAMs functionalized electrodes. b,c) Semilogarithmic and

linear plot of I_{ds} vs V_{gs} transfer curves at a fixed bias voltage (V_{ds}) of 5 V. d-f) I_{ds} vs V_{ds} output curves at a step V_{gs} from -90 V to 90 V with a 30 V intervals. g-i) Statistical distribution of the linear mobility of top-contact FETs devices with functionalized and unfunctionalized electrodes.

To investigate the electrical properties of the SAMs modified top-contact electrodes on the carrier injection, we measured the transfer and output characteristics for the unfunctionalized, PFBT functionalized, and DABT functionalized MoS_2 FETs under nitrogen environment (Figure 2). For the sake of comparison, channel length and width normalized current ($I = I_{ds}\frac{L}{W}$) of MoS_2 FETs as a function of back-gated voltage (V_{gs}) are displayed in Figure 2b and 2c, where I_{ds} is the source drain current, and L/W is the length/width ratio of the channel. Figure 2d-f shows the typical output curves of devices. Table S1 summarizes the extracted electrical parameters of these devices. The non-ohmic "S" shape of the output characteristics at lower bias indicates an obvious Schottky barrier in the carrier injection region.[9,27] With the increasing bias voltage, the contact between the electrode and MoS_2 displays ohmic-like behavior. The devices comprising unfunctionalized Au electrode exhibit transfer curves typical for electron transport in MoS_2 FETs with a threshold voltage (V_{th}) of 7.1 V, which is in contrast to the p-type behavior of previous studies.[4] This is mainly attributed to substrate induced doping and the appreciable roughness of the electrode surface.[18,21a] The statistical distribution and average values of the apparent linear mobility (μ) are depicted in Figure 2g-i and table S1. The best performance was obtained for the device with DABT treated electrode with the average μ values of 30.6 ± 8.8 $cm^2\ V^{-1}\ s^{-1}$. While the devices with bare Au electrode exhibit moderate performance with the average μ values of 16.9 ± 5.2 $cm^2\ V^{-1}\ s^{-1}$ and the FET containing the PFBT treated electrode exhibit degraded performance with the average μ values of 8.1 ± 3.6 $cm^2\ V^{-1}\ s^{-1}$. As a result, compared with bare gold electrodes, DABT treated electrodes facilitate the charge injection thus improving the device performance, while PFBT-treated electrodes suppress it. Moreover, these results also exhibit better performance than the bottom-contact configuration.[9]

Besides the relevance of the field-effect mobility, the threshold voltage engineering is also important towards the device performance optimization.[28] As shown in Figure 3h, DABT functionalized electrodes display a significant negative shift of V_{th} (-21.4 V) and an apparent increase of I_{ds} without augmenting the hysteresis, evidencing the n-doping of MoS_2. From the V_{th} shift, the change of charge carrier densities (Δn) can be estimated (see formula S2 in the Supporting Information). The quantified Δn amounts to 1.08×10^{12} cm^{-2}, being a value comparable to those observed when using traditional n-dopants.[29] On the other hand, a clear

positive shift of V_{th} (11.0 V) and a substantial decrease of the overall current is obtained upon PFBT functionalized electrodes also without increasing the hysteresis, evidencing a p-doping effect. The estimated Δn amounts to $-5.54 \times 10^{11}\,\mathrm{cm^{-2}}$, in line with reported molecular p-dopants.[29c,30] However, a previous report by Cho et al.[31] demonstrated that the contact region modification with thiolated molecules of any type can be instrumental to improve device performance by reducing the injection tunneling barrier and by creating additional tunneling percolation pathways. This is because thiol molecules had been directly deposited on the flake surface and chemically adsorbed at the sulfur vacancies of MoS_2 by generating a covalent bond with Mo atoms. The healed and repaired sulfur vacancy defects bring about the elimination of interface states and the improvement of overall performance.[32] It is reported that defects on the surface of MoS_2 can be utilized to control the device electrical behavior.[33] Moreover, the thermally evaporated Au with MoS_2 interface is degenerately doped, which is different from the transferred Au.[21b] Our results above based on the top-contact configuration clearly revealed that in absence of chemical functionalization of the MoS_2, the increase of the WF of Au electrode yields a significant degradation of the device electrical performance. This also suggests that SAMs functionalization of top-electrode is an efficient way to control carrier transport in MoS_2 transistors. Significantly, the possibility of transferring metal electrodes functionalized with appropriate SAMs makes it possible to tune the device performance with a high precision.

To further evaluate the impacts of SAMs functionalized electrode on the charge injection, we extracted the SBH by using the following thermionic emission equation:[23a,34]

$$I_{ds} = AA^{*}T^{2}\exp\left(-\frac{\Phi_{SB}}{k_B T}\right)\exp\left(\frac{qV_{ds}}{k_B T}\right) \tag{4}$$

$$\Phi_{SB} = -k_B\left[\frac{\mathrm{d}\ln(I_{ds}/T^2)}{\mathrm{d}(1/T)}\right] \tag{5}$$

where A is the junction area, A^{*} is the equivalent Richardson constant, k_B is the Boltzmann constant and T is temperature. The Φ_{SB} is the slope of a linear fit to $\ln(I_{ds}/T^2)$ as a function of $1/T$, equation 5. In this way, the Φ_{SB} under various gate voltages and the effective Φ_{SB} (under the flat-band condition) can be obtained. Figure S6-S8 show the temperature dependent transfer characteristics of MoS_2 transistors with bare Au electrode and SAMs functionalized electrodes. The extracted Φ_{SB} at various gate voltages for all devices are shown in figure 3a-c. As can be seen, the effective Φ_{SB} amounts to 0.19, 0.07 and 0.53 eV for bare Au electrode, DABT and PFBT functionalized electrode, respectively. The extracted effective Φ_{SB} for various electrodes

as a function of the corresponding work functions are displayed in Figure 3i. The dash line is the linear fitting with a slope indicating a pinning factor (S) of 0.33. The value is much larger than the previously reported values of 0.02~0.11 for deposited metals, and better than metal oxide interlayer of 0.24.[6a,23a] This confirms that metal electrodes functionalized with various SAMs can be used to alleviate FLP and tune the SBH of multilayered MoS_2 FETs.

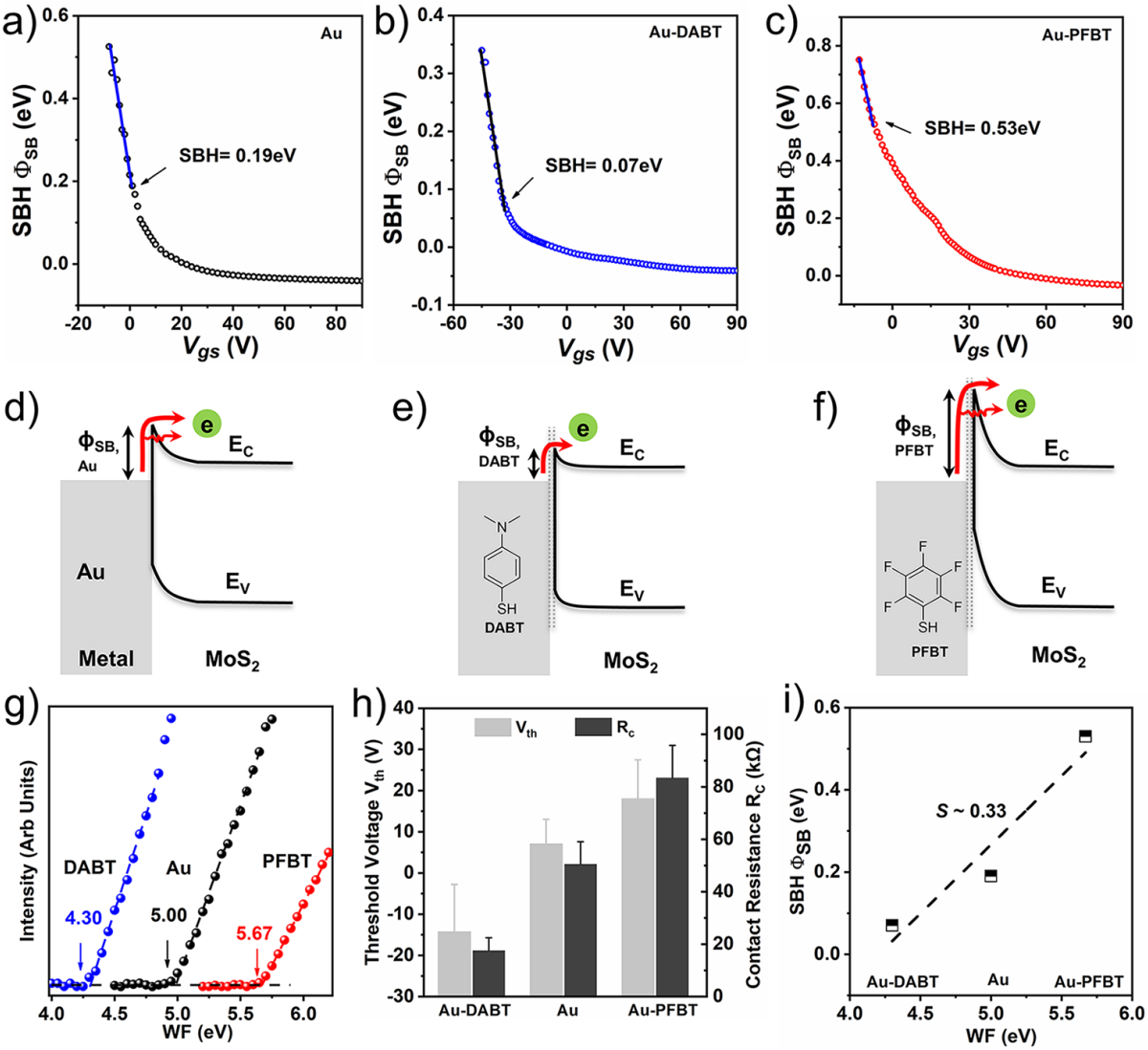

Figure 3. a-c) Extracted SBH values at various gate voltages for MoS_2 FETs with functionalized and unfunctionalized electrodes. d-f) Energy band diagrams for multilayer MoS_2 crystal contacted with bare gold electrode (e), DABT (d) and PFBT (f) functionalized gold electrode. The red arrows represent the different injection mechanisms. From top to bottom: thermionic emission, field emission (tunneling).[35] The gray dotted line represents the molecular spacing. g) Secondary electron cutoff of DABT functionalized (blue dots) and PFBT functionalized (red dots) Au electrodes compared to the corresponding unfunctionalized Au electrodes (measures by PYSA, see Instrumentation in Supporting Information). h) Threshold voltage V_{th} and contact resistance R_C of FETs devices for the bare Au, DABT, and PFBT functionalized electrodes cases.

i) Experimentally determined effective electron SBH as a function of work function for the bare Au, DABT and PFBT functionalized electrode cases.

Figure 3d-f illustrate the mechanism of SAMs functionalized electrode on the charge injection. Interfacial charge transfer process takes place upon deposition of the electrodes onto the semiconducting MoS_2 flake. For device based on bare Au electrodes (figure 3d), a Φ_{SB} of 0.19 eV was reported. As shown in figure 3e, the functionalization with DABT molecules determines a decrease in the WF (4.30 eV) significantly reducing the Φ_{SB} hence promoting carrier injection from electrode to semiconductor, thereby overall improving the device performance. On the contrary, the PFBT functionalized electrode (5.67 eV) displays a major enhancement in the Φ_{SB}, worsening the electron injection at the electrode-semiconductor interface, hence yielding an overall degradation of the device electrical characteristics (figure 3f). In addition, figure 3h shows the contact resistance (R_C) of the various devices which was evaluated by using Y-function method, being an established protocol for evaluating R_C in organic materials and TMDs semiconductor based FETs.[36] Detailed information regarding the Y-function method are provided in the Supporting Information. The extracted R_C values amounts to 17.6 ± 4.8, 50.6 ± 8.5, and 83.5 ± 12.3 $k\Omega$ for DABT functionalized, Au unfunctionalized, and PFBT functionalized electrodes in top-contact MoS_2 FETs, respectively. The estimated width-normalized R_C resulted 66.2 ± 33.8, 144.8 ± 33.1, and 337.8 ± 166.2 $k\Omega \cdot$ µm, respectively. These findings are consistent with the trends of μ and V_{th}, and are in line with previous reports.[31,35]

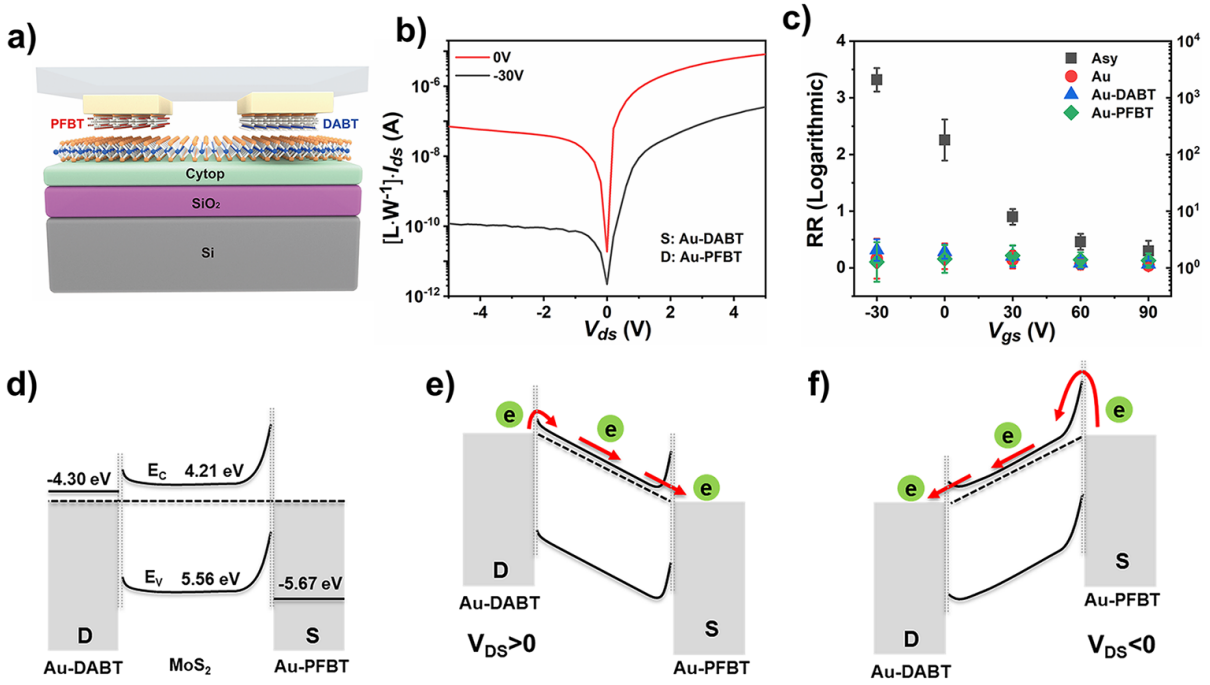

Figure 4. (a) Schematic illustration of asymmetric MoS_2 FETs device. (b) Semilogarithmic plot of the I_{ds}– V_{ds} output curve at 0 V and -30 V gate bias conditions. The drain electrode is PFBT functionalized electrode and the DABT functionalized electrode is grounded. (c) Rectification ratio at V_{ds} in different gate bias conditions. d-f) Energy band diagram of asymmetric MoS_2 FETs devices. (d) Energy band diagram at thermodynamic equilibrium. The black lines show the original WF energy of DABT and PFBT functionalized electrode. (e) Energy band diagram at positively biased source-drain condition. (f) Energy band diagram at negatively biased source-drain condition.

By taking the method a step further, it is also possible to transfer pairs of diversely SAMs functionalized electrodes to introduce electronic asymmetry in the device thereby enabling the fabrication of Schottky diodes. Figure 4a shows the schematic cartoon of the metal–semiconductor–metal (MSM) Schottky diode produced by transferring DABT and PFBT functionalized electrodes as vdW contacts. The $I_{ds} - V_{ds}$ output characteristics of Schottky diode as a function of V_{gs} are reported in figure 4b and figure S9. The use of DABT and PFBT functionalized asymmetric electrodes yielded a decrease of the V_{gs} from 90 V to -30V, with a significant increase in the rectification ratio (RR) reaching a maximum value of 10^3 at the V_{gs} of -30 V, as shown in figure 4c, which is comparable to the diodes produced using asymmetric metal or oxidized metal contacts.[37] This can be understood that negative V_{gs} shifts the energy bands upward, which results in the increase in the injection barrier. With the increasing of V_{gs}, the energy bands were shifted downward, which makes the channel more conductive, and an increased current is observed. At strong accumulation region, the barriers on both sides are negligible and the RR becomes uniform.[37a] Figure 4d reports a scheme of the energy band diagrams for functionalized asymmetric electrodes MoS_2 FETs. As aforementioned, the WF of the DABT and PFBT functionalized Au electrodes are different. Once the electrodes are in contact with the semiconductor, the charge will flow from the semiconductor to the Fermi level of the electrodes, thereby forming different space charge regions on both two contact areas of the semiconductor surface, which also results in different injection barrier heights for the DABT and PFBT functionalized electrodes (Figure 4d). When the DABT functionalized electrode is grounded, the carriers can be injected through a lower barrier from DABT functionalized electrode into semiconductor (Figure 4e) when a positive V_{ds} is applied. Conversely, when a negative V_{ds} is applied, the carriers must overcome a higher barrier to be injected from PFBT functionalized electrode into the semiconductor (Figure 4f), yielding a poored electron injection and lower currents, leading to a rectification.[31,36d]

In summary, we have reported for the first time on the integration of chemically functionalized source and drain electrodes in top-contact MoS_2 FETs by using the dry transfer

technique. We have demonstrated that the SAMs functionalized electrodes in top-contact configuration can significantly modulate the performance of FETs by choosing commercially available thiol molecules with different dipoles moment. In perfect agreement with the theoretical prediction, the electrodes functionalization determines a reduction of the injection barrier which yields in and efficient improvement of the device performance. Furthermore, we have upgraded this approach to enable the asymmetric functionalization of source and drain electrodes that resulted in the fabrication of high-performance Schottky diodes. This technique not only eliminates the influence of bottom electrode modification on the semiconductor by enhancing the area of injection, but also offers a viable approach for the functionalization of top electrodes for tuning the device characteristics. The work we presented here thus demonstrated a generally applicable functionalized metal integration strategy for the construction of high-performance staggered 2D semiconductor based FETs, which can be extended to other delicate functional materials, such as organic single crystal or thin-film semiconductors, and to other applications in which asymmetry is required like planar inverters, light-emitting devices and solar cells.

Experimental Section

Experimental details are available in the Supporting Information.

Supporting Information

Supporting Information is available from the Wiley Online Library or from the author.

Acknowledgements

This work is supported by the EC through the ERC project SUPRA2DMAT (GA-833707) and the Graphene Flagship Core 3 project (GA-881603) as well as the Labex projects CSC (ANR-10LABX-0026 CSC) and NIE (ANR-11-LABX-0058 NIE) within the Investissement d'Avenir program ANR-10-IDEX-0002-02 the International Center for Frontier Research in Chemistry, the Institut Universitaire de France (IUF) and the Chinese Scholarship Council.

Received: ((will be filled in by the editorial staff))
Revised: ((will be filled in by the editorial staff))
Published online: ((will be filled in by the editorial staff))

Conflict of Interest

The authors declare no conflict of interest.

References

[1] a) B. Radisavljevic, A. Radenovic, J. Brivio, V. Giacometti, A. Kis, *Nat. Nanotechnol.* **2011**, *6*, 147; b) K. F. Mak, C. Lee, J. Hone, J. Shan, T. F. Heinz, *Phys. Rev. Lett.* **2010**, *105*, 136805; c) A. M. Jones, H. Yu, N. J. Ghimire, S. Wu, G. Aivazian, J. S. Ross, B. Zhao, J. Yan, D. G. Mandrus, D. Xiao, W. Yao, X. Xu, *Nat. Nanotechnol.* **2013**, *8*, 634; d) M. Chhowalla, D. Jena, H. Zhang, *Nat. Rev. Mater.* **2016**, *1*, 16052.

[2] a) H. Liu, A. T. Neal, P. D. Ye, *ACS Nano* **2012**, *6*, 8563; b) M. Choi, Y. J. Park, B. K. Sharma, S. R. Bae, S. Y. Kim, J. H. Ahn, *Sci. Adv.* **2018**, *4*, s8721.

[3] a) S. Casalini, C. A. Bortolotti, F. Leonardi, F. Biscarini, *Chem. Soc. Rev.* **2017**, *46*, 40; b) A. Liscio, E. Orgiu, J. M. Mativetsky, V. Palermo, P. Samorì, *Adv. Mater.* **2010**, *22*, 5018; c) S. Bertolazzi, M. Gobbi, Y. Zhao, C. Backes, P. Samorì, *Chem. Soc. Rev.* **2018**, *47*, 6845; d) Y. Yao, Y. Chen, H. Wang, P. Samorì, *SmartMat* **2020**, *1*, e1009; e) D. S. Schulman, A. J. Arnold, S. Das, *Chem. Soc. Rev.* **2018**, *47*, 3037.

[4] Y. Liu, J. Guo, E. Zhu, L. Liao, S.-J. Lee, M. Ding, I. Shakir, V. Gambin, Y. Huang, X. Duan, *Nature* **2018**, *557*, 696.

[5] P.-C. Shen, C. Su, Y. Lin, A.-S. Chou, C.-C. Cheng, J.-H. Park, M.-H. Chiu, A.-Y. Lu, H.-L. Tang, M. M. Tavakoli, G. Pitner, X. Ji, Z. Cai, N. Mao, J. Wang, V. Tung, J. Li, J. Bokor, A. Zettl, C.-I. Wu, T. Palacios, L.-J. Li, J. Kong, *Nature* **2021**, *593*, 211.

[6] a) G.-S. Kim, S.-H. Kim, J. Park, K. H. Han, J. Kim, H.-Y. Yu, *ACS Nano* **2018**, *12*, 6292; b) J. Wang, Q. Yao, C.-W. Huang, X. Zou, L. Liao, S. Chen, Z. Fan, K. Zhang, W. Wu, X. Xiao, C. Jiang, W.-W. Wu, *Adv. Mater.* **2016**, *28*, 8302; c) S. Chuang, C. Battaglia, A. Azcatl, S. McDonnell, J. S. Kang, X. Yin, M. Tosun, R. Kapadia, H. Fang, R. M. Wallace, A. Javey, *Nano Lett.* **2014**, *14*, 1337; d) X. Cui, E.-M. Shih, L. A. Jauregui, S. H. Chae, Y. D. Kim, B. Li, D. Seo, K. Pistunova, J. Yin, J.-H. Park, H.-J. Choi, Y. H. Lee, K. Watanabe, T. Taniguchi, P. Kim, C. R. Dean, J. C. Hone, *Nano Lett.* **2017**, *17*, 4781; e) S. McDonnell, A. Azcatl, R. Addou, C. Gong, C. Battaglia, S. Chuang, K. Cho, A. Javey, R. M. Wallace, *ACS Nano* **2014**, *8*, 6265.

[7] S.-S. Chee, D. Seo, H. Kim, H. Jang, S. Lee, S. P. Moon, K. H. Lee, S. W. Kim, H. Choi, M.-H. Ham, *Adv. Mater.* **2019**, *31*, 1804422.

[8] Y. Zhao, K. Xu, F. Pan, C. Zhou, F. Zhou, Y. Chai, *Adv. Funct. Mater.* **2017**, *27*, 1603484.

[9] A. Matković, A. Petritz, G. Schider, M. Krammer, M. Kratzer, E. Karner-Petritz, A. Fian, H. Gold, M. Gärtner, A. Terfort, C. Teichert, E. Zojer, K. Zojer, B. Stadlober, *Adv. Electron. Mater.* **2020**, *6*, 2000110.

[10] a) T. Li, J. W. Balk, P. P. Ruden, I. H. Campbell, D. L. Smith, *J. Appl. Phys.* **2002**, *91*, 4312; b) D. Gupta, M. Katiyar, D. Gupta, *Org. Electron.* **2009**, *10*, 775; c) C. Shim, F. Maruoka, R. Hattori, *IEEE Trans. Electron Devices* **2010**, *57*, 195; d) A. Herasimovich, S. Scheinert, I. Hörselmann, *J. Appl. Phys.* **2007**, *102*, 054509; e) S. Scheinert, G. Paasch, *J. Appl. Phys.* **2009**, *105*, 014509; f) M. N. Islam, B. Mazhari, *IEEE Trans. Electron Devices* **2014**, *61*, 4204.

[11] D. J. Gundlach, L. Zhou, J. A. Nichols, T. N. Jackson, P. V. Necliudov, M. S. Shur, *J. Appl. Phys.* **2006**, *100*, 024509.

[12] a) D. Natali, M. Caironi, *Adv. Mater.* **2012**, *24*, 1357; b) M. Waldrip, O. D. Jurchescu, D. J. Gundlach, E. G. Bittle, *Adv. Funct. Mater.* **2020**, *30*, 1904576; c) J. Youn, G. R. Dholakia, H. Huang, J. W. Hennek, A. Facchetti, T. J. Marks, *Adv. Funct. Mater.* **2012**, *22*, 1856; d) L. Han, Y. Huang, W. Tang, S. Chen, J. Zhao, X. Guo, *J. Phys. D: Appl. Phys.* **2019**, *53*, 014002; e) C.-a. Di, Y. Liu, G. Yu, D. Zhu, *Acc. Chem. Res.* **2009**, *42*, 1573.

[13] a) H. Haick, D. Cahen, *Acc. Chem. Res.* **2008**, *41*, 359; b) C. R. Hansen, T. J. Sørensen, M. Glyvradal, J. Larsen, S. H. Eisenhardt, T. Bjørnholm, M. M. Nielsen, R. Feidenhans'l, B. W. Laursen, *Nano Lett.* **2009**, *9*, 1052.

[14] a) Z. Xu, S.-H. Li, L. Ma, G. Li, Y. Yang, *Appl. Phys. Lett.* **2007**, *91*, 092911; b) H. Kleemann, K. Krechan, A. Fischer, K. Leo, *Adv. Funct. Mater.* **2020**, *30*, 1907113.

[15] S. Gowrisanker, Y. Ai, M. A. Quevedo-Lopez, H. Jia, H. N. Alshareef, E. Vogel, B. Gnade, *Appl. Phys. Lett.* **2008**, *92*, 153305.

[16] A. Petritz, M. Krammer, E. Sauter, M. Gärtner, G. Nascimbeni, B. Schrode, A. Fian, H. Gold, A. Cojocaru, E. Karner-Petritz, R. Resel, A. Terfort, E. Zojer, M. Zharnikov, K. Zojer, B. Stadlober, *Adv. Funct. Mater.* **2018**, *28*, 1804462.

[17] a) Q. Tang, L. Jiang, Y. Tong, H. Li, Y. Liu, Z. Wang, W. Hu, Y. Liu, D. Zhu, *Adv. Mater.* **2008**, *20*, 2947; b) Q. Tang, Y. Tong, H. Li, Z. Ji, L. Li, W. Hu, Y. Liu, D. Zhu, *Adv. Mater.* **2008**, *20*, 1511.

[18] a) B. Liu, W. Zhao, Z. Ding, I. Verzhbitskiy, L. Li, J. Lu, J. Chen, G. Eda, K. P. Loh, *Adv. Mater.* **2016**, *28*, 6457; b) G. Yoo, S. L. Choi, S. Lee, B. Yoo, S. Kim, M. S. Oh, *Appl. Phys. Lett.* **2016**, *108*, 263106.

[19] D. Jariwala, V. K. Sangwan, D. J. Late, J. E. Johns, V. P. Dravid, T. J. Marks, L. J. Lauhon, M. C. Hersam, *Appl. Phys. Lett.* **2013**, *102*, 173107.

[20] B. Han, Y. Li, X. Ji, X. Song, S. Ding, B. Li, H. Khalid, Y. Zhang, X. Xu, L. Tian, H. Dong, X. Yu, W. Hu, *J. Am. Chem. Soc.* **2020**, *142*, 9708.

[21] a) L. Liu, L. Kong, Q. Li, C. He, L. Ren, Q. Tao, X. Yang, J. Lin, B. Zhao, Z. Li, Y. Chen, W. Li, W. Song, Z. Lu, G. Li, S. Li, X. Duan, A. Pan, L. Liao, Y. Liu, *Nat. Electron.* **2021**, *4*, 342; b) K. Jo, P. Kumar, J. Orr, S. B. Anantharaman, J. Miao, M. J. Motala, A. Bandyopadhyay, K. Kisslinger, C. Muratore, V. B. Shenoy, E. A. Stach, N. R. Glavin, D. Jariwala, *ACS Nano* **2021**, *15*, 5618.

[22] P. Stoliar, R. Kshirsagar, M. Massi, P. Annibale, C. Albonetti, D. M. de Leeuw, F. Biscarini, *J. Am. Chem. Soc.* **2007**, *129*, 6477.

[23] a) C. Kim, I. Moon, D. Lee, M. S. Choi, F. Ahmed, S. Nam, Y. Cho, H.-J. Shin, S. Park, W. J. Yoo, *ACS Nano* **2017**, *11*, 1588; b) J. Bardeen, *Phys. Rev.* **1947**, *71*, 717.

[24] a) C. Liu, Y. Xu, Y.-Y. Noh, *Mater. Today* **2015**, *18*, 79; b) G. Heimel, L. Romaner, E. Zojer, J.-L. Bredas, *Acc. Chem. Res.* **2008**, *41*, 721; c) C. M. Bowers, D. Rappoport, M. Baghbanzadeh, F. C. Simeone, K.-C. Liao, S. N. Semenov, T. Żaba, P. Cyganik, A. Aspuru-Guzik, G. M. Whitesides, *J. Phys. Chem. C* **2016**, *120*, 11331.

[25] a) L. Kankate, T. Hamann, S. Li, L. V. Moskaleva, A. Gölzhäuser, A. Turchanin, P. Swiderek, *Phys. Chem. Chem. Phys.* **2018**, *20*, 29918; b) S. Li, D. Guérin, S. Lenfant, K. Lmimouni, *AIP Adv.* **2018**, *8*, 025110.

[26] C. Vericat, M. E. Vela, G. Benitez, P. Carro, R. C. Salvarezza, *Chem. Soc. Rev.* **2010**, *39*, 1805.

[27] F. Ante, D. Kälblein, T. Zaki, U. Zschieschang, K. Takimiya, M. Ikeda, T. Sekitani, T. Someya, J. N. Burghartz, K. Kern, H. Klauk, *Small* **2012**, *8*, 73.

[28] a) J. Roh, J. H. Ryu, G. W. Baek, H. Jung, S. G. Seo, K. An, B. G. Jeong, D. C. Lee, B. H. Hong, W. K. Bae, J.-H. Lee, C. Lee, S. H. Jin, *Small* **2019**, *15*, 1803852; b) Y. Kim, S. Chung, K. Cho, D. Harkin, W.-T. Hwang, D. Yoo, J.-K. Kim, W. Lee, Y. Song, H. Ahn, Y. Hong, H. Sirringhaus, K. Kang, T. Lee, *Adv. Mater.* **2019**, *31*, 1806697; c) Y. Zhao, S. Bertolazzi, P. Samorì, *ACS Nano* **2019**, *13*, 4814; d) Y. Zhao, S. Bertolazzi, M. S. Maglione, C. Rovira, M. Mas-Torrent, P. Samorì, *Adv. Mater.* **2020**, *32*, 2000740.

[29] a) Y. Wang, A. Slassi, J. Cornil, D. Beljonne, P. Samorì, *Small* **2019**, *15*, 1903432; b) Y. Wang, A. Slassi, M.-A. Stoeckel, S. Bertolazzi, J. Cornil, D. Beljonne, P. Samorì, *J. Phys. Chem. Lett.* **2019**, *10*, 540; c) Y. Li, C.-Y. Xu, P. Hu, L. Zhen, *ACS Nano* **2013**, *7*, 7795.

[30] a) D. M. Sim, M. Kim, S. Yim, M.-J. Choi, J. Choi, S. Yoo, Y. S. Jung, *ACS Nano* **2015**, *9*, 12115; b) D.-H. Kang, M.-S. Kim, J. Shim, J. Jeon, H.-Y. Park, W.-S. Jung, H.-Y. Yu, C.-H. Pang, S. Lee, J.-H. Park, *Adv. Funct. Mater.* **2015**, *25*, 4219; c) H. Liu, D. Grasseschi, A. Dodda, K. Fujisawa, D. Olson, E. Kahn, F. Zhang, T. Zhang, Y. Lei, N. Branco Ricardo Braga, L. Elías Ana, C. Silva Rodolfo, Y.-T. Yeh, M. Maroneze Camila, L. Seixas, P. Hopkins, S. Das, J. S. de Matos Christiano, M. Terrones, *Sci. Adv.* **2020**, *6*, eabc9308.

[31] K. Cho, J. Pak, J.-K. Kim, K. Kang, T.-Y. Kim, J. Shin, B. Y. Choi, S. Chung, T. Lee, *Adv. Mater.* **2018**, *30*, 1705540.

[32] a) Z. Yu, Y. Pan, Y. Shen, Z. Wang, Z.-Y. Ong, T. Xu, R. Xin, L. Pan, B. Wang, L. Sun, J. Wang, G. Zhang, Y. W. Zhang, Y. Shi, X. Wang, *Nat. Commun.* **2014**, *5*, 5290; b) S. Ippolito, A. G. Kelly, R. Furlan de Oliveira, M.-A. Stoeckel, D. Iglesias, A. Roy, C. Downing, Z. Bian, L. Lombardi, Y. A. Samad, V. Nicolosi, A. C. Ferrari, J. N. Coleman, P. Samorì, *Nat. Nanotechnol.* **2021**, *16*, 592; c) M. Farmanbar, G. Brocks, *Adv. Electron. Mater.* **2016**, *2*, 1500405.

[33] a) S. Bang, S. Lee, A. Rai, N. T. Duong, I. Kawk, S. Wolf, C.-H. Chung, S. K. Banerjee, A. C. Kummel, M. S. Jeong, J. H. Park, *Adv. Funct. Mater.* **2020**, *30*, 2000250; b) F. Giannazzo, G. Fisichella, G. Greco, S. Di Franco, I. Deretzis, A. La Magna, C. Bongiorno, G. Nicotra, C. Spinella, M. Scopelliti, B. Pignataro, S. Agnello, F. Roccaforte, *ACS Appl. Mater. Interfaces* **2017**, *9*, 23164; c) D. Liu, Y. Guo, L. Fang, J. Robertson, *Appl. Phys. Lett.* **2013**, *103*, 183113.

[34] A. Anwar, B. Nabet, J. Culp, F. Castro, *J. Appl. Phys.* **1999**, *85*, 2663.

[35] A. Allain, J. Kang, K. Banerjee, A. Kis, *Nat. Mater.* **2015**, *14*, 1195.

[36] a) G. Ghibaudo, *Electron. Lett.* **1988**, *24*, 543; b) K.-C. Lee, S.-H. Yang, Y.-S. Sung, Y.-M. Chang, C.-Y. Lin, F.-S. Yang, M. Li, K. Watanabe, T. Taniguchi, C.-H. Ho, C.-H. Lien, Y.-F. Lin, *Adv. Funct. Mater.* **2019**, *29*, 1809011; c) S.-J. Choi, P. Bennett, K. Takei, C. Wang, C. C. Lo, A. Javey, J. Bokor, *ACS Nano* **2013**, *7*, 798; d) Y. Zhao, X. Xiao, Y. Huo, Y. Wang, T. Zhang, K. Jiang, J. Wang, S. Fan, Q. Li, *ACS Appl. Mater. Interfaces* **2017**, *9*, 18945.

[37] a) A. Di Bartolomeo, A. Grillo, F. Urban, L. Iemmo, F. Giubileo, G. Luongo, G. Amato, L. Croin, L. Sun, S.-J. Liang, L. K. Ang, *Adv. Funct. Mater.* **2018**, *28*, 1800657; b) H. S. Yoon, H.-E. Joe, S. Jun Kim, H. S. Lee, S. Im, B.-K. Min, S. C. Jun, *Sci. Rep.* **2015**, *5*, 10440; c) M. Hussain, S. Aftab, S. H. A. Jaffery, A. Ali, S. Hussain, D. N. Cong, R. Akhtar, Y. Seo, J. Eom, P. Gautam, H. Noh, J. Jung, *Sci. Rep.* **2020**, *10*, 9374.